Proceedings of the RAAD 2008
17th International Workshop on Robotics in Alpe–Adria–Danube Region
September 15-17, 2008, Ancona, Italy

Experimental Error in Measuring Temperature-Induced Deformation in a Single-Link System

Pranchalee Poonyapak [a], J. Moyra J. McDill [b] and M. John D. Hayes[b]

Mechanical and Aerospace Engineering, Carleton University, Canada

[a]*E-mail: ppoonyap@connect.carleton.ca*
[b]*E-mail: {mmcdill, jhayes}@mae.carleton.ca*
URL: www.mae.carleton.ca

Abstract.
Temperature-induced deformation has been observed to occur during the warm-up cycle of industrial robots. To enable robots to do productive work during the warm-up time it is necessary to compensate for temperature-induced dimensional deformation. As a step in this direction, the development of single-link experimental models and the resolution of problems relating to experimental procedures to measure dimensional deformation are presented. A single-link mechanical system is subject to applied heat. A thermal imaging camera records the time-dependent temperature history of the link. Longitudinal and transverse changes in link dimension are made by tracking the change in location of the geometric centroid of a spot projected on a CCD camera chip by a laser diode rigidly fixed to the distal end of the link. Multiple sources of measurement error are identified by comparing the experimental results to transient thermal-mechanical finite element analysis (FEA), and simple analytical models. Experimental results reveal the relative magnitude of the contribution of each source of error, and methods are used to attenuate the errors. The most significant errors are shown to be related to the extraction of the sub-pixel coordinates of the laser spot centroid, as well as thermal effects of the CCD camera. Results from the improved experimental setup show very close agrement between the link deformation measurement and FEA predictions. These results give sufficient confidence in the experimental setup to be certain of deformation measurements on the order of 10 μm. The combined experimental, numerical, and analytical work will support the development of a motion control algorithm which compensates for temperature-induced deformation.

Keywords. Temperature-induced dimensional deformation; warm-up cycle time; measurement error; transient heat transfer; thermal and dimensional steady state.

1. Introduction

An often overlooked issue in serial robots is that repeatability and accuracy may not be constant throughout the entire volume of the workspace and they can vary over time (ISO, 1998). Fluctuations arise from temperature-induced deformations, responses to applied loads, dynamic characteristics and system errors in the controller inverse kinematics.

Temperature-induced deformation appears to be particularly critical during the warm-up cycle (Poonyapak et al., 2007). The thermal instability results from the losses in the robot motors and typically requires a period of continuous motion through the workspace to establish steady state (ISO, 1998). The long term goal of the current research is to develop an analytical model-based control algorithm to compensate for the thermal deformation that occurs during the warm-up period, thereby

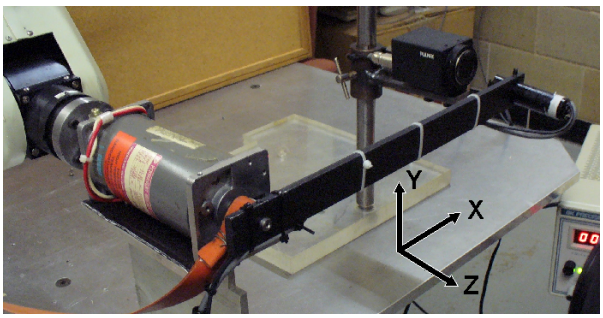

Fig. 1. Experimental apparatus (Poonyapak et al., 2007)

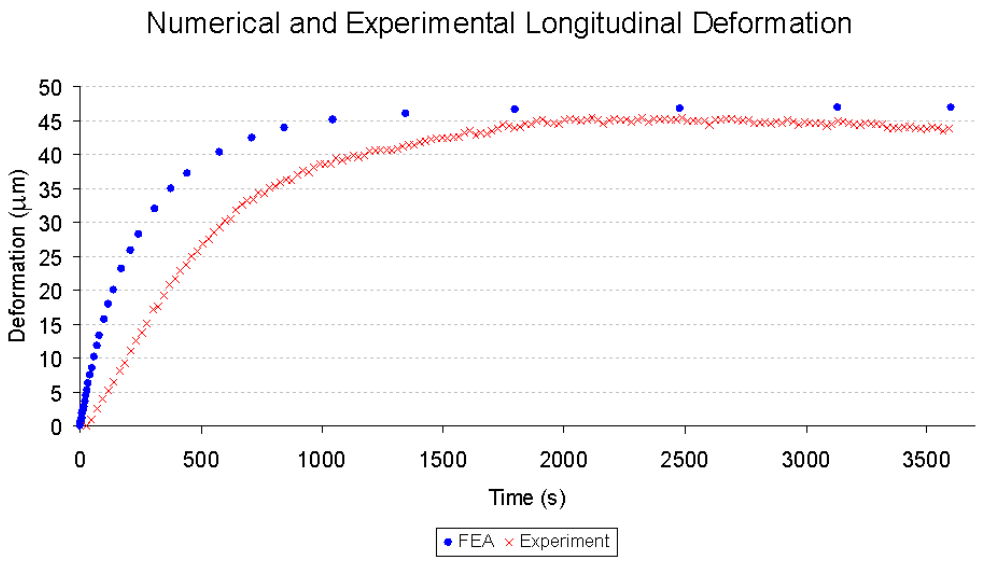

Fig. 2. Longitudinal deformation - numerical and experimental results at the laser diode for the moving link case (Poonyapak et al., 2007)

increasing productivity and reducing unnecessary energy consumption.

The work presented in this paper employs a combination of simplified experimental, numerical (finite element analysis, FEA), and analytical models. This allows cross-calibration and checking of the experimental, numerical and analytical results. Eventually, a refined analytical model will be used for motion control. In this paper, the authors consider the development of the experimental models and the resolution of problems relating to the experiment procedures.

In a previous study of a simplified single-link robot mechanical system (Poonyapak et al., 2007), experimental, numerical (FEA) and analytical data were obtained for both stationary and moving link cases. The experimental model incorporated a single-link mechanical system and an optical measurement system. The single-link system comprised a slender aluminum link attached to the shaft of a servo motor manipulated by the tool flange of a Thermo CRS A465 robot. Temperature measurements were obtained using an infrared camera. Longitudinal deformation measurements were obtained by tracking the drift of the spot from a laser diode, rigidly mounted to the distal end of the link, across a stationary CCD camera chip. The experimental setup is shown in Fig. 1.

While the temperature distribution results showed good agreement between the experimental and FEA results at steady state[1], this was not the case for the longitudinal deformation results. Fig. 2 shows two significant differences in the temperature-induced longitudinal deformation of the robot geometry between FEA (predicted) and experimental (measured) results were observed particularly in the moving link case. The FEA results reach steady state faster and have a higher steady state deformation when compared to the experiment. At steady state, the difference is about 3.5%, as shown in Fig. 2. It was unclear whether the differences were caused by experimental apparatus and/or procedures, by assumptions made in the FEA, e.g., boundary conditions, or both. However, a number of uncertainties in the experimental apparatus suggested that it was the more likely source of the differences.

[1]The FEA model, including material properties and boundary conditions is reported and discussed in detail in Poonyapak et al. (2007).

2. Evaluation of the Experimental Models

An examination of the experimental setup identified a number of potential sources of error as listed in Tab. 1. The effects related to the linkage include bending, linkage alignment, dimensional deformation of the diode hole in the link, and movement of the diode. The effects related to the robot and heating pad are robot idle-induced vibration, which may vibrate the link-diode assembly, and the use of a stiff heating pad which may contribute to non-uniform heating. In terms of the measurement system, thermal deformation of the camera mounting plate must be considered as well as the accuracy of estimating the sub-pixel coordinates of the laser spot through the centroid extraction algorithm and concerns about laser spot size.

Tab. 1. Potential sources of error

Area of experiment	Topic	Results		
		analytical	experimental	numerical
6061Al link	Effects of cantilever bending.	√	–	–
	Effects of link alignment.	√	–	–
	Expansion of diameter of the diode hole and movement of the diode.	√	–	√
Robot model	Robot idle-induced vibration.	–	√	–
	Flexibility of heating pad.	–	√	–
Measurement method	Effects of accuracy of laser centroid extraction.	–	√	–
	Thermal effects of CCD camera.	–	√	–

For each topic listed in Tab. 1, information was available from at least one of the analytical, numerical or experimental results. Analytical analysis showed that the first three items listed would produce relatively insignificant effects. Work then focussed on the robot model and the measurement system. The remaining concerns were considered in turn addressing first the stationary link case and concluding with a moving link experiment.

2.1. Robot Idle-Induced Vibration

In the single-link experiment (Poonyapak et al., 2007), the link was well fastened to the drive shaft which, in turn, was rigidly fastened to the robot tool flange through a coupling piece. The drive shaft and link can be considered a rigid body. In the stationary experiment, the link did not move. Despite this, the experimental results showed a consistent trend of a low amplitude oscillation of the centroid of the laser beam in the y-axis (transverse) direction. The oscillation is believed to be caused by idle-induced vibration of the robot.

To isolate the effects of the robot idle-induced vibration from the system, the experimental setup needs to be decoupled from the robot. The drive shaft was disconnected from the robot and the link assembly was then fastened directly to the workbench. The single-link experiment was repeated with the vibration-isolated setup. To reduce other factors that might mask the effects of the vibration, the heating pad was not used.

Fig. 3 shows the experimental results of the vibration-isolated experiment superimposed on those of the regular-setup experiment using increments of equal size. The locations of the centroid of the laser spot in both longitudinal and transverse directions, with and without idle vibration, are plotted over a 100-minute period.

Fig. 3(a) shows that the vibration has an effect on the measurement in the x-axis (longitudinal) direction. The amplitude of the oscillation of the centroid location changes from approximately ± 0.20 μm with idle-induced vibration to ± 0.18 μm over the 100-minute period. However, it is not clear if this difference is caused

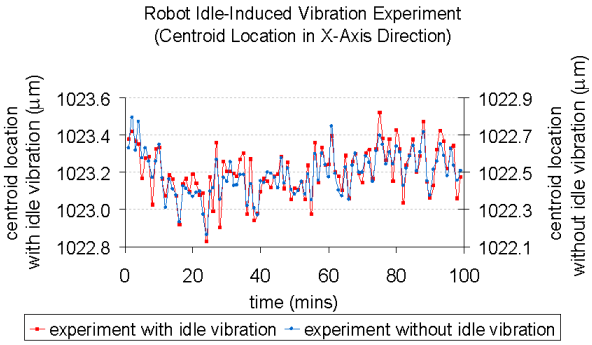

(a) Centroid location in x-axis (longitudinal) direction.

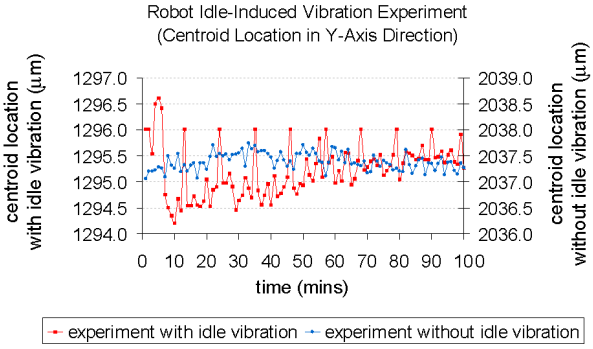

(b) Centroid location in y-axis (transverse) direction.

Fig. 3. Results of robot idle-induced experiment for the stationary link case

exclusively by the idle vibration. In the transverse direction, as seen in Fig. 3(b), the effects are more obvious. The amplitude of the oscillation of the centroid location changes from approximately ± 1.5 μm to ± 0.3 μm over the 100-minute period, while the amplitude remains constant at approximately ± 0.25 μm without the effects of the vibration. That is, the amplitude of the vibration at the start is almost eight times bigger than that of the non-effected case. These results are summarized in Tab. 2.

Idle-induced vibration can be eliminated in practice

Tab. 2. Accuracy improvement due to centroid extraction algorithm

Measurement direction	Idle-induced vibration	Amplitude of oscillation (μm)	Average % amplitude reduction
X-axis	√	±0.20	10%
	-	±0.18	
Y-axis	√	decreasing from ±1.5 to ±0.30	16% - 416%
	-	±0.25	

by turning off the robot controller when running a stationary link experiment. Note that in the moving link case, the robot idle-induced vibration is not an issue since the robot is in motion and does not idle.

2.2. Flexibility of heating pad

The temperature results obtained from the infrared (IR) camera during the single-link experiment (Poonyapak et al., 2007) suggested that the heating pad could be a possible source of error in temperature measurement. Initially, a 25.4 mm × 300 mm silicone rubber, fibreglass insulated heater was used to supply heat to the drive shaft of the system. The large width and thickness of the heating pad did not allow it to be snugly wrapped completely around the exposed surface of the shaft. The heating pad was instead rolled into a loose hoop around the shaft as shown in Fig. 4. With the small contact area between the heating pad and the drive shaft, concentrated heat was applied to the drive shaft at only discrete locations. It was noted that changes in the position of the heating pad location, especially in the moving link case experiment where the shaft rotated, could occur since it was not permanently mounted on the shaft.

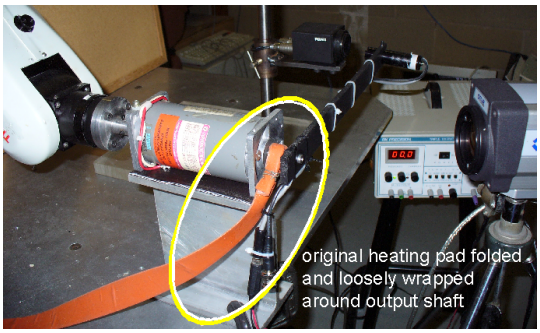

Fig. 4. Original heating pad assembled on drive shaft

The original heating pad was replaced by a Kapton insulated flexible heater, which has a very small thickness (0.25 mm). This 100 mm long heating pad was then tightly wrapped around the length of the drive shaft with thin twine.

As seen in the temperature results in Fig. 5, the average temperature in the area around the heating pad is 23.5°C. The increase of temperature from the initial temperature of the same area is only 1.5°C, which is approximately 65% lower than the 4°C increase when using the old heating pad. With this improved arrangement, particularly the elimination of unused heating pad length, consistent heating was provided to the linkage in both the stationary and moving link cases. Additionally, the heat convection to the air in the vicinity of the drive shaft was significantly reduced.

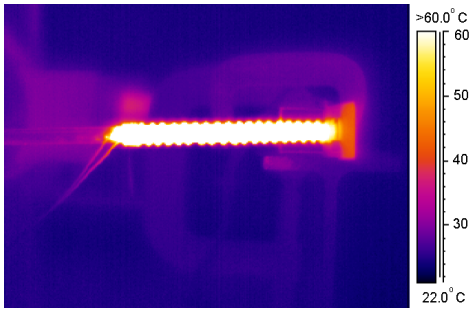

Fig. 5. IR image of new heating pad affixed to the drive shaft

(a) Small laser spot. (b) Large laser spot.

Fig. 6. Images of laser spot taken by CCD camera

2.3. Effects of accuracy of laser centroid extraction

In the discussion of robot idle-induced vibration, it was shown that idle-induced vibration is one of the sources of the oscillation appearing in the plot of the locations of the centroid of the laser spot in the y-axis direction. When the setup is isolated from the vibration, the oscillation amplitude is reduced, but not completely elimi-

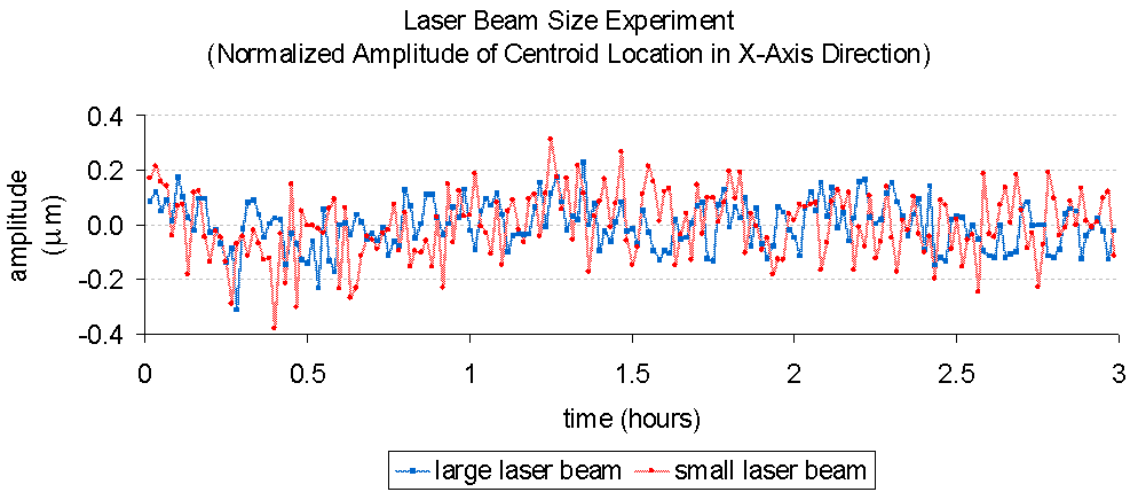

Fig. 7. Results of laser spot size experiment for the stationary link case

Tab. 3. Accuracy improvement due to centroid extraction algorithm

Modification method	Standard deviation of experimental results (μm)		% improvement
	before modification	after modification	
Modified algorithm	0.1433	0.1002	30%
Large laser spot	0.1221	0.0878	28%

nated. This points out that there are more sources of the oscillation that need to be identified to improve the accuracy of the results. The accuracy of the laser centroid sub-pixel coordinate extraction from images acquired by the CCD camera potentially affects the accuracy of the overall experimental results (Vincze et al., 1994). Two possible improvements are modification of the geometric centroid extraction algorithm, and the adjustment of laser spot size used in the experiment. As will be shown, both improvements used in tandem provide the best results to date.

Laser spot geometric centroid extraction algorithm Each grayscale image of the laser spot obtained from the CCD camera is evaluated by the algorithm coded in Matlab to compute the sub-pixel coordinates of the geometric centroid of the laser spot. Each pixel in the image of the laser spot contains a 16-bit grayscale colour value corresponding to the intensity of the laser at the specific location. The colour scale ranges from black to white, and is evenly divided. Each shade is assigned a value between 0 (black) and 65535 (white)[2]. The location of the geometric centroid of the laser spot is found using a method similar to determining the centre of gravity of an object with mass moment about the x- and y-axes (Leitner et al., 2001). Each colour-defined value is then analogous to a weighted fraction of the system mass.

In the original extraction algorithm, all pixels were evaluated. It was noted that the image of the laser spot was not as bright and sharp and appeared as a blurred gray circle instead of a sharp white one. The low intensity of the pixels around the edge of the laser spot was not always consistent. Hence, even small changes of intensity on a small number of pixels affected the overall accuracy of the centroid extraction algorithm.

To address the inconsistency of the intensity of the laser spot periphery, the algorithm was modified to allow the user to set a threshold value of the lowest intensity to be used for each extraction. Any shades of gray that represent a lower intensity of the laser spot than the threshold will be considered black. This improves the accuracy of the extraction algorithm.

Laser spot size adjustment In the robot repeatability experiment (Leitner et al., 2001) performed prior to the single-link experiment (Poonyapak et al., 2007), it was assumed that the extraction algorithm would be more accurate if the laser spot was tuned to be as fine as possible, i.e., close to being invisible. This assumption was based on the theory that a smaller area spot would impose less computational error in the extraction of the sub-pixel coordinates of the geometric centroid of the illuminated

[2] $2^{16} - 1$.

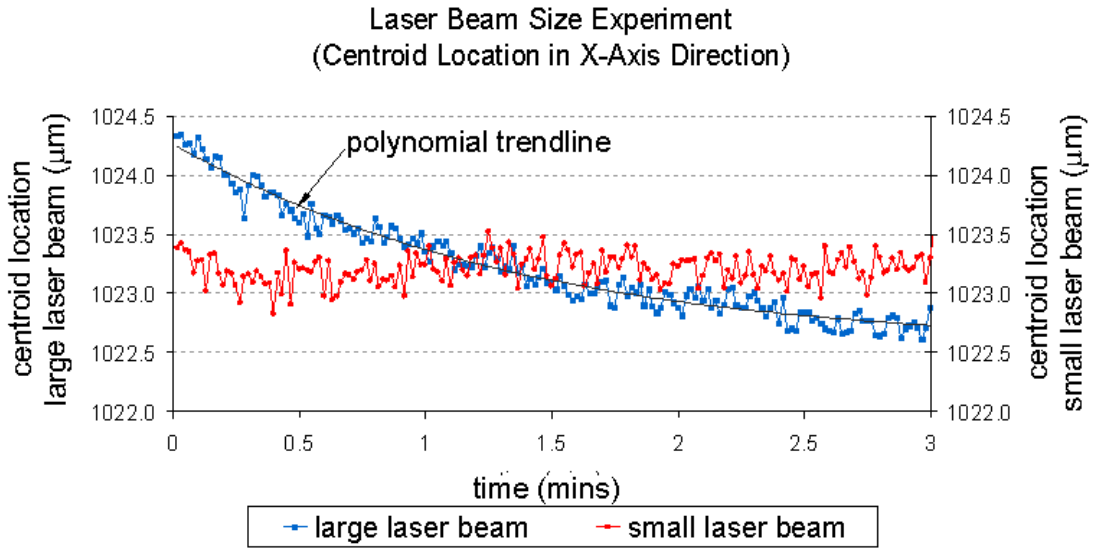

Fig. 8. Results of the laser spot size experiment for the stationary link case before normalizing

area. This assumption was also applied to the single-link experiment (Poonyapak et al., 2007). However, the requirements of the repeatability experiment (Leitner et al., 2001) are different than those of this application. As is shown below, testing revealed that for this application the centroid extraction algorithm would yield superior estimates if the moments were distributed over a larger number of pixels. This is because the computation of the coordinates of the centroid of a larger area spot is affected less than that of a smaller area spot when there are fluctuations in spot area. Such fluctuations arise from low intensity pixels on the periphery being filtered out by the threshold limit. The use of a large laser spot increases the number of white pixels, decreases the number of intermediate intensity level (non-black) pixels and thereby improves the accuracy of the geometric centroid extraction algorithm.

Fig. 6(a) is a sample of the original near-invisible laser spot. In the new approach, the laser spot was tuned and focused so its shape was an ellipsoid with shape parameters approaching that of a sharp-edged circle, e.g. Fig. 6(b). Typically the size of the laser spot circle with the sharpest edge was found to be approximately 10 times larger than when the spot was tuned to be almost invisible. The acquisition parameters of the CCD camera are set in Labview to be more sensitive to the differences of the pixel intensity levels to detect the laser spot edge.

Combined Effects In investigating the effects of the laser spot size and the quality of the laser spot image for the modified geometric centroid extraction algorithm, the voltage reference levels of black and white were set to be 0.6 and 0.7 V respectively. Fig. 7 shows the superimposed amplitude plots of the centroid location in the longitudinal direction, normalized by the magnitude of the mean values of the small and large laser spot centroid locations in the x-axis direction over a period of 3 hours. The range of the oscillations seen with the large laser spot is less than that of the small laser spot. This implies greater accuracy for the sub-pixel coordinate estimation. Note, in Fig. 7 the data were normalized to remove the effects of thermal expansion of the CCD camera stand (see Subsection 2.4).

A summary of the improvements using the modified geometric centroid extraction algorithm is presented in Tab. 3. Separately, the modified algorithm and the use of a larger laser spot might provide as much as a 30% improvement in the estimation of the longitudinal deformation. The improved level of confidence in the results applies to both the stationary and moving cases, but depends on the quality of laser spot images.

2.4. Thermal effects of the CCD camera

In studying the effects of laser spot centroid extraction, it was noted that the position of the large diameter laser spot centroid changed with time as shown in Fig. 8. The resulting polynomial trend was unexpected and indicated an obvious source of error. Fig. 9 shows the temperature data obtained while examining the effects of laser spot size. It can be seen that some of heat generated by the CCD camera was transferred to the camera mounting plate. Any thermal expansion occurring at the aluminum mounting plate will, in turn, alter the measurements made with the CCD camera.

The aluminum mounting plate is 101.6 mm long (L),

25.4 mm wide and 6.2 mm thick and has a linear coefficient of thermal expansion (α) of $23.6 \times 10^{-6} K^{-1}$ (6061 Al). Obtained from thermal images such as Fig. 9, the initial and steady state temperatures (T_0 and T_i respectively) of the mounting plate are 22°C and 25.5°C. Using the standard equation for linear thermal expansion, i.e. $\Delta L = \alpha L|Ti - To|$, the change in length in the longitudinal direction is 2.05 μm. This compares to the corresponding change, extracted from Fig. 8, of 1.90 μm. The difference of nearly 8% suggests that the thermal deformation of the mounting plate is in itself a dominant source of measurement error.

To reduce the thermal effects of the CCD camera, three modifications to the experimental setup, and one modification to the experimental procedure were made. First, a 4 mm thick rubber gasket was inserted between the CCD camera and the mounting plate to decrease the amount of heat transferred to the stand by conduction. Second, a piece of mineral wool insulation was placed between the back of the camera and the post to reduce any effects of convection heating to the post. Third, fins were attached to the CCD camera to help release the heat to the environment. Finally, in the experimental procedure, better results were obtained when the CCD camera was warmed-up before performing experimental tasks. The data suggest that the camera will reach steady state after 30 minutes of continuous operation. Fig. 10(a) illustrates the mounting plate. Figs. 10(b) and 10(c) show the camera stand before and after applying the improvements to the setup. The single-link experiment was then repeated with the modified setup with and without applied heat. For the case when heat was applied, the system was initially at room temperature then the drive shaft was heated. To ensure that thermal steady state was reached and the cooling effects were completely separated from the heating effects, the heating pad was left on for approximately two hours after steady state was first detected at 50 minutes. The heating pad was then turned off and both temperature and deformation data were recorded for another 100 minutes.

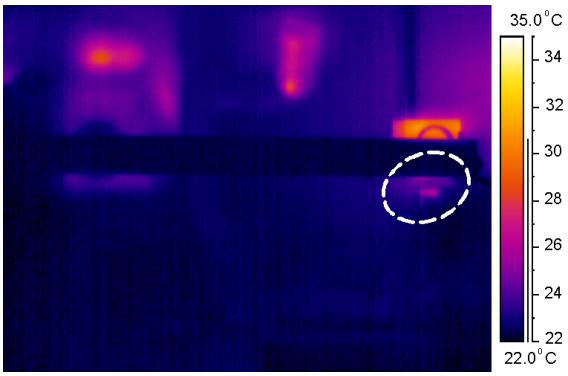

Fig. 9. Heated CCD camera stand

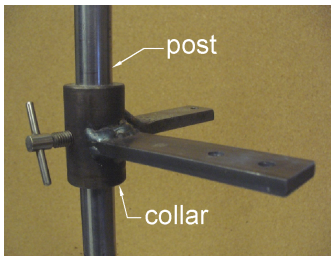

(a) Mounting plate.

(b) Original setup.

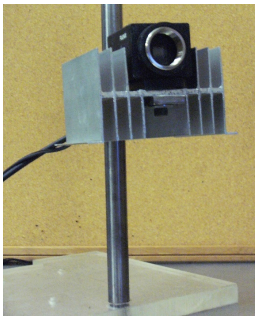

(c) modified setup.

Fig. 10. Camera stand

Fig. 11 shows the temperature results at the CCD camera of the thermal-effect-isolated experiment with no heat applied. With the modified setup, the temperature increase of the mounting plate was reduced from 3.5°C to 2°C when compared to the original setup. This is nearly a 40% improvement. It can also be seen that the temperature of the air around the CCD camera was greater (26°C vs 24.5°C) with the modified setup.

Fig. 12(a) shows the location of the centroid of the laser spot in the x-axis for the experiment when no heat is applied. In the absence of applied heat the change in centroid location is nil. Fig. 12(b) illustrates the change in location of the laser spot centroid due to the increase in temperature of the link from room temperature after the application of heat. Steady state is reached at about 50 minutes, after which the centroid location remains stable until cooling begins. The detected deformation, in this case, is 10 μm. The system required approximately 50

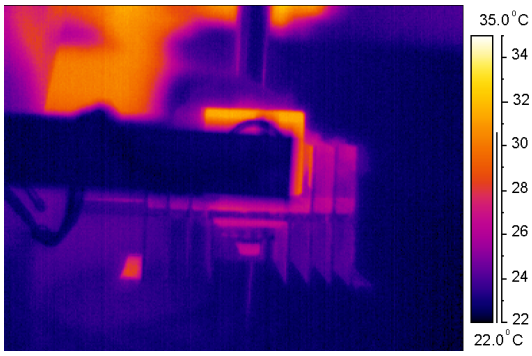

Fig. 11. Temperature results of thermal-effect experiment with no applied heat

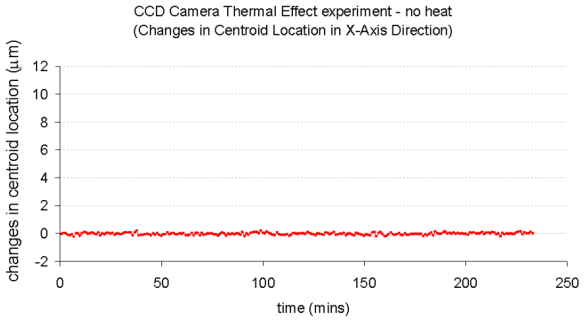

(a) Experiment with no heat applied.

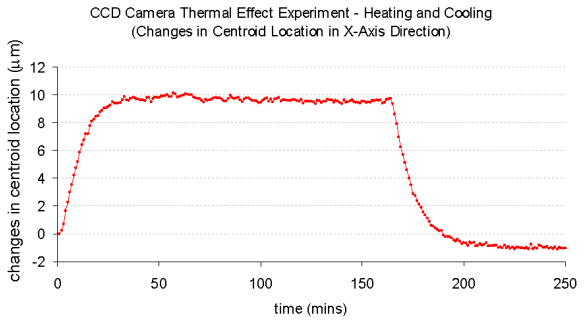

(b) Experiment with heating and cooling periods.

Fig. 12. Deformation results of thermal-effect experiment

minutes for both heating up and cooling down periods [3].

With the modified setup, the centroid locations are no longer affected by thermal expansion of the aluminium mounting plate. The polynomial behaviour seen in Fig. 8 is thereby eliminated. In Fig. 12(b) it is seen that the variation in deformation at steady state is approximately $\pm 0.15\ \mu$m. This is several orders of magnitude smaller than the overall expected longitudinal deformation of 40 to 100 μm and provides a sufficient measurement resolution. The stability of results in Fig. 12(b) recorded over the period of approximately 125 minutes also provides sufficient confidence in the experimental setup to be certain of deformation measurements on the order of 10 μm. While these experiments were performed using the stationary link case, it is clear that the results also apply to the moving link case.

3. Discussion

The goal of this paper has been to identify and eliminate experimental sources of error which cause discrepancies between observed experimental results and FEA predictions of longitudinal deformation in a simplified robot mechanical system. Of particular concern was that the FEA results reached steady state faster than the experimental results and had a higher steady state deformation when compared to the experiment.

As a final step, all experimental changes were employed in a moving link experiment. In this particular experiment a greater, and more demanding, heat input was applied to the system. Fig. 13 shows that the longitudinal deformation from the experiment and the FEA model now have good agreement in both the rise time response and the value of deformation at steady state when compared to Fig. 2. The most significant improvements in the experimental results arose from changes in the approach to extraction of the laser spot centroid location as it migrates across the CCD chip, as well as elimination of the thermal effects of the CCD camera.

A new heating pad has also been installed to provide more uniform and consistent heat input. It is also important to prevent any physical disturbance to the laser diode. For stationary link experiments the effects of the idle-induced vibration can be eliminated by turning off the robot controller. A study is underway to examine the FEA model, in particular the boundary conditions associated with the varying natural convection conditions which may be present in the laboratory.

Having addressed the potential sources of error, there is now sufficient confidence in the experimental setup to be certain of deformation measurements on the order of 10 μm. This, in turn, makes it possible to proceed to a multi-link mechanical system and to develop a motion control algorithm based on a refined analytical model.

4. Conclusions

A number of problems relating to experimental procedures and the sources of measurement error in estimating the temperature-induced deformation of a single-link

[3] The difference in the start and end centroid locations is the result of a higher initial temperature associated with the previous experimental run.

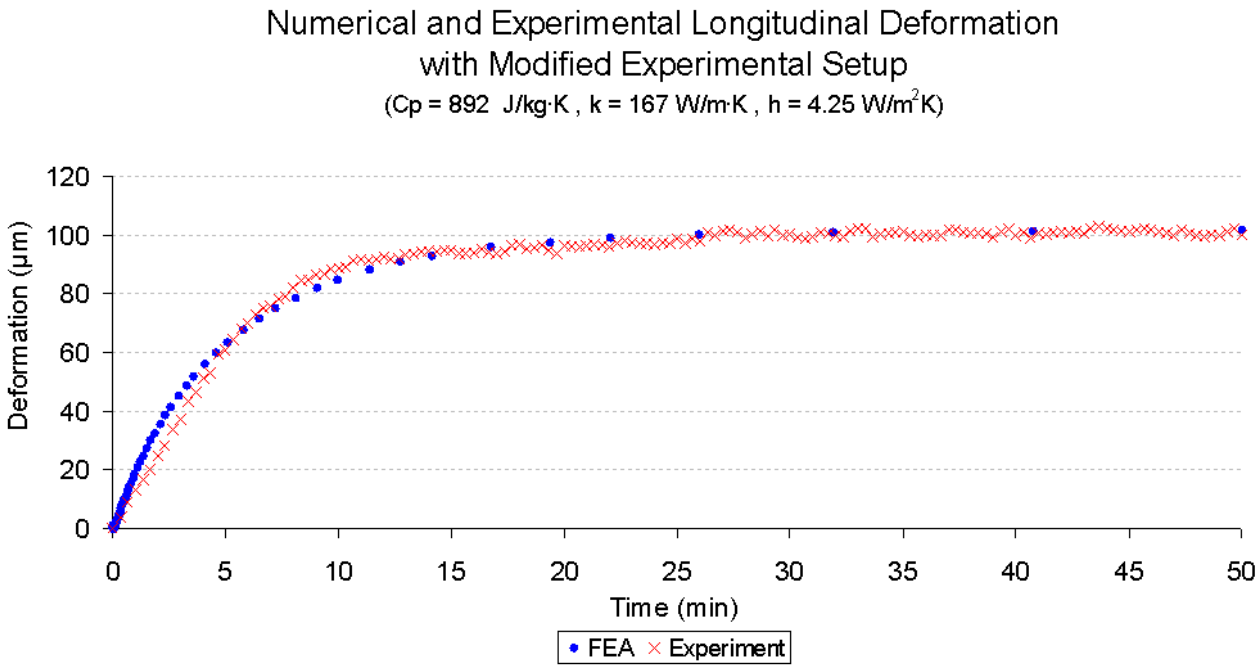

Fig. 13. Longitudinal deformation - numerical and experimental results using modified experimental setup for the moving link case

robot mechanical system have been resolved. The results indicate that the most significant improvements resulted from changes in the extraction of the laser spot centroid location, as well as elimination of the thermal effects of the CCD camera. There is now sufficient confidence in the experimental setup to be certain of deformation measurements on the order of 10 μm. A motion control algorithm based on a refined analytical model will be tuned using material properties and boundary conditions established in the new multi-link FEA models in support of continued experimental measurements.

5. Acknowledgments

The authors wish to acknowledge the financial support of NSERC grants 41745 and 250012.

6. References

ISO 9283:1998(E) Manipulating industrial robots - Performance criteria, and related test methods. 1998. 2nd Edition.

Leitner, M., Hayes, M.J.D., Ofner, R., Sallinger, C., O'Leary, P. 2001. Thermal Effects and Consequences for Repeatability of an industrial Robot. In: *Proc. 18th Canadian Congress of Applied Mechanics*, St. John's, Canada, June.

Poonyapak, P., Hayes, M.J.D., McDill, J.M.J. 2007. Temperature-Induced Deformation in a Mechanical System. In: *Proc. 12th IFToMM World Congress*, Besancon, France, June 17-21.

Vincze, M., Prenniger, J., Gander, H.. 1994. A Laser Tracking System to Measure Position and Orientation of Robot End Effectors under Motion, *International Journal of Robotics Research*, 13(4): 305-314, 1994.